

# PCCP

Accepted Manuscript



This is an *Accepted Manuscript*, which has been through the Royal Society of Chemistry peer review process and has been accepted for publication.

*Accepted Manuscripts* are published online shortly after acceptance, before technical editing, formatting and proof reading. Using this free service, authors can make their results available to the community, in citable form, before we publish the edited article. We will replace this *Accepted Manuscript* with the edited and formatted *Advance Article* as soon as it is available.

You can find more information about *Accepted Manuscripts* in the [Information for Authors](#).

Please note that technical editing may introduce minor changes to the text and/or graphics, which may alter content. The journal's standard [Terms & Conditions](#) and the [Ethical guidelines](#) still apply. In no event shall the Royal Society of Chemistry be held responsible for any errors or omissions in this *Accepted Manuscript* or any consequences arising from the use of any information it contains.

# The role of water co-adsorption on the modification of ZnO nanowires with acetic acid

Adriel Domínguez,<sup>\*‡</sup> Svea grosse Holthaus,<sup>‡</sup> Susan Köppen, Thomas Frauenheim and Andreia Luisa da Rosa

Received Xth XXXXXXXXXXXX 20XX, Accepted Xth XXXXXXXXXXXX 20XX

First published on the web Xth XXXXXXXXXXXX 200X

DOI: 10.1039/b000000x

Density functional theory (DFT) and Car-Parinello molecular dynamic simulations were employed to investigate the interaction of acetic acid with nonpolar facets of ultra-thin ZnO nanowires. We consider both a dry and a water environment as well as different molecule coverages for the hydrated system. Our calculations reveal that the fully-covered nanowire is energetically favored in aqueous environment at room temperature. We also identified a minor influence of liquid water on the denticity of the ligands for the fully modified system. On the other hand, a monodentate adsorption is expected for a half-covered nanowire due to strong ligand-water interactions.

## 1 Introduction

For the increasing demand to develop a sustainable and green nano-technology, the fabrication of nanostructure-based devices with high integration densities has gained importance as it requires less source material than conventional layer-based approaches. Nanostructured materials have large surface-to-volume ratios which offers a unique possibility of enhancing sensitivity and selectivity. Chemical species introduced onto the surface of such nanostructures could then be employed to create novel hybrid functional devices. Charge accumulation or depletion in one-dimensional nanostructures can take place in the bulk region of the structure, which gives rise to large changes in their electrical properties. Such feature is particularly desirable for efficient charge injection in solar cells. In particular, one-dimensional nanostructures such as nanowires are preferable, since they naturally provide a direct path for electrical transport. Experiments reveal that electron transport can be up to two orders of magnitude faster in nanowire-based dye-sensitized solar cells (DSSC) than in nanoparticle DSSCs<sup>1–3</sup>.

Currently, hybrid organic-inorganic solar cells have a relatively low efficiency (below 10%) and limited stability. These factors strongly depend on the structural details of the organic-inorganic interface which includes binding mechanisms, band offsets and electron injection. Due to the complexity of the interface an explicit theoretical understanding at the atomistic level can help unveiling the limiting factors and consequently

enhancing the device performance.

In DSSCs the organic dye molecules usually attach to the oxide surface via one or several functional groups. The nature of the exposed surface planes of the oxide and the mode of interaction with the organic molecule is the first important information to understand. For example, in the adsorption of the N3 dye on TiO<sub>2</sub> anatase (101) surfaces, the sensitizer binds through two of the four carboxyl groups (-COOH), at least one of them being anchored via a bidentate configuration bridging two adjacent titanium sites<sup>4</sup>. However, there are still controversies on how the geometry of these molecules on the oxide surfaces and the character of this interaction (physisorption versus chemisorption) affects the electronic and optical properties of the hybrid material<sup>5–7</sup>.

Although TiO<sub>2</sub> has become the semiconductor material of choice for the preparation of DSSCs, ZnO-based solar cells have been increasingly investigated.<sup>2,8–15</sup> ZnO represents an appealing alternative to TiO<sub>2</sub> due to its promising transport properties and the possibility of fabrication of an ample variety of ZnO nanostructures. However, the highest efficiencies accomplished with ZnO-based DSSCs are still considerably smaller than for TiO<sub>2</sub>-based cells.<sup>16,17</sup> In this sense, a better understanding of the dye-ZnO interface and in particular, the interaction of ZnO with the employed anchoring groups, may be crucial for the design of solar cells with improved efficiency.

Among the compounds employed for the functionalization of ZnO surfaces and nanostructures, carboxylic acids have emerged as one of the most promising choices.<sup>5,18–25</sup> However, there seems to be a general discrepancy about the success of -COOH as an anchor group for this metal oxide. Whereas some measurements suggest a favorable covalent binding of

Bremen Center for Computational Material Science, University of Bremen, Am Fallturm 1, 28359, Bremen, Germany.

E-mail: [adrieltg@bccms.uni-bremen.de](mailto:adrieltg@bccms.uni-bremen.de)

<sup>‡</sup> These authors contributed equally to this work.

the functional group on ZnO nanostructures,<sup>5,23,24,26</sup> other studies indicate surface etching under certain experimental circumstances.<sup>27</sup> Especially, pH conditions must be carefully controlled to prevent that the ZnO structures undergo unwanted reactions in the presence of carboxylic acid. Theoretical investigations have demonstrated the stability of -COOH group on ZnO surfaces in gas phase<sup>28–30</sup>. In a previous work<sup>29</sup> we pointed out that the stability of acetic acid (AcOH) [employed as prototype adsorbate to study the interaction of -COOH with ZnO] on nonpolar ZnO surfaces remains even in a water environment for moderate concentrations of the ligand. This conclusion was drawn from purely thermodynamic considerations. The explicit inclusion of water in the hybrid system is however fundamental to gain more insight into these phenomena.

In this paper we investigate the adsorption of AcOH on the surfaces of ZnO nanowires under both dry and aqueous conditions by employing Density functional theory (DFT) and Car-Parinello molecular dynamic simulations. The aqueous case is simulated by specific addition of bulk water in our model.

## 2 Model and computational details

The bare nanowires have been modeled by cutting a hexagonal prism out of a ZnO wurzite structure in such a way that their growth direction is oriented along the *c*-axis and they exhibit non-polar (10 $\bar{1}$ 0) and (1 $\bar{2}$ 10) facets as shown in Figure 1. For all systems we considered a tetragonal supercell with a dimension of  $30 \times 30 \times 5.41 \text{ \AA}^3$ , containing 48 atoms and a large vacuum region so that no spurious interaction with the nanowire replicas takes place. The lattice parameter *c* for the bare structure was optimized and kept fixed for every subsequent calculation. We define the molecular coverage on the nanowire  $\theta$  as the number of AcOH molecules adsorbed per surface Zn-O pair. For the AcOH-covered nanowire in a dry environment, we consider adsorption of the molecules on every available binding site, which corresponds to  $\theta = 1$ . This amounts to 12 molecules per supercell.

The initial molecular geometries correspond to the preferred configurations found in a previous investigation on the adsorption of AcOH on non-polar surfaces<sup>29</sup>. It should be noticed that the (10 $\bar{1}$ 0) surface is invariant under a reflection about a perpendicular (1 $\bar{2}$ 10) plane containing the zinc binding sites ( $Zn_A$  in Fig 1). Additionally, as AcOH is an achiral compound, bend molecular configurations with orientations to one or the other direction along the normal to the (1 $\bar{2}$ 10) plane are equivalent. We chose alternate orientation of the molecules in such a way that on a same (10 $\bar{1}$ 0) facet they look in the same direction whereas the orientation is switched in the neighboring (10 $\bar{1}$ 0) facets. This in turn implies that at the (1 $\bar{2}$ 10) facets they are either oriented towards or opposing each other. In this way, every second (1 $\bar{2}$ 10) facet displays a *ligand-free* region

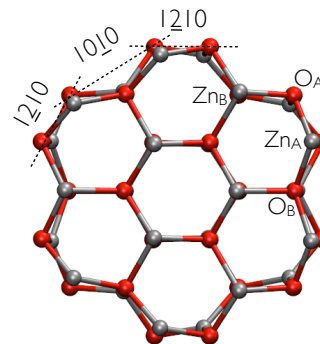


**Fig. 1** Cross-sectional view of the optimized structure of the bare ZnO nanowire. Zinc (oxygen) atoms are displayed by silver (red) spheres.

which has been explicitly flagged with black arrows in Figure 2. We will come back to this point later. It is obviously possible to build up a system with all molecules oriented toward the same direction. However, the chosen model allows us to study two possible scenarios regarding the ligand adsorption while considering a single adduct configuration.

For the geometry optimization, DFT calculations were performed as implemented in the Vienna ab initio Simulation Package (VASP) code<sup>31–34</sup>. The Kohn-Sham equations were solved using the generalized gradient approximation (GGA) with the Perdew-Burke-Ernzerhof (PBE) form for the exchange-correlation functional<sup>35,36</sup>. Plane wave basis sets with a cutoff energy of 300 eV as well as the projector-augmented wave (PAW) method<sup>37,38</sup> have been employed. For the integration in the Brillouin zone, a  $(1 \times 1 \times 4)$  Monkhorst-Pack *k*-point sampling<sup>39,40</sup> was conducted. During the calculations, all atoms were allowed to move till the interatomic forces were smaller than  $10^{-2} \text{ eV/\AA}$ .

Molecular Dynamic (MD) simulations were performed using Car-Parinello MD as implemented in the CPMD code.<sup>41</sup> We used *ab-initio* ultrasoft-pseudopotentials to describe the atomic potentials<sup>42</sup>. The plane wave cutoff energy was set to 30 Ryd (300 Ryd) for the electronic wavefunctions (charge density). For all MD simulations the Brillouin zone integration was performed using the  $\Gamma$ -point only. The equations of motion were integrated using a timestep of 5 a.u. and an electron mass of 300 a.u. All systems were heated up to 300 K using a Nose-Hoover thermostat applying a heating figure in which the temperature is held constant at values of 40, 70, 120, and 200 K for 500 integration steps<sup>43</sup>. The region between the periodically repeated nanowires was filled with water molecules up to a density of about  $1 \text{ g/cm}^3$  which corresponds to 124 water molecules per supercell. Molecular coverages of  $\theta = 0, 0.5$  and 1 were considered.

### 3 Results

#### 3.1 Geometry and binding energies under dry conditions

Previous results show that AcOH dissociates on ZnO nonpolar surfaces as one hydrogen atom migrates from the -COOH group to the surface oxygen site<sup>28,29</sup>. Our results regarding the adsorption on the nanowire support this dissociative regime. The molecule was also found to relax to a bidentate chelating mode in a similar manner as reported for the surface, as seen in Figure 2. To have insight into the strength of the adsorbate-substrate interaction and compare it with previous results for the surface, we calculated the adsorption energy per ligand. This quantity is defined as

$$E_{\text{ads}} = \frac{1}{n}(E_{\text{T}} - E_{\text{bare}} - nE_{\text{AcOH}}), \quad (1)$$

where  $E_{\text{T}}$  is the total energy of the modified nanowire,  $E_{\text{bare}}$  is the total energy of the bare nanowire,  $E_{\text{AcOH}}$  is the energy of an isolated neutral AcOH molecule in gas phase and  $n$  is the number of molecules adsorbed on the nanowire. The obtained adsorption energy of AcOH on the ZnO nanowire is -1.31 eV, which compares well to the adsorption energy of AcOH on the surface which is -1.39 eV.<sup>29</sup>

The relaxation of nanowire facets upon adsorption of AcOH also resembles that observed for the ZnO surfaces. The surface Zn atoms relax outwards, thus enlarging the bond length of  $\text{Zn}_A\text{-O}_A$  surface pairs. In this case, the bond length goes from 1.90 Å for the bare nanowire to 2.04-2.12 Å for the modified nanostructure, for a relative elongation of up to 12%. This value is slightly greater than the 9% enlargement found for the two-dimensional model. At the same time, the bond lengths between the four-fold coordinated  $\text{Zn}_B$  and the  $\text{O}_A$  atoms in the modified nanowire experience a reduction of around 6% with respect to the bare wire. Hydrogen bonds with one of the -COOH oxygens have bond lengths of 1.66 Å. Previous DFT-based tight-binding calculations for the interaction of AcOH with the (1010) ZnO surface reported a somewhat larger value of 1.74 Å.<sup>28</sup> The C-O bond lengths of the -COOH group vary from 1.31 to 1.27 Å. This is in agreement with the findings for the (1010) surface.

#### 3.2 Geometry and adsorption energies in aqueous environment

Our discussion has so far been limited to the adsorption of AcOH in a dry environment. We now turn to a more realistic model by including bulk water in the AcOH/ZnO system. This model is suitable as a first approximation to investigate the stability of the modified nanowire in a wet environment. The optimized structure for the adsorption in the dry environment was chosen as initial configuration of the adsorbate. To analyze the influence of the aqueous media on the ligand adsorption,

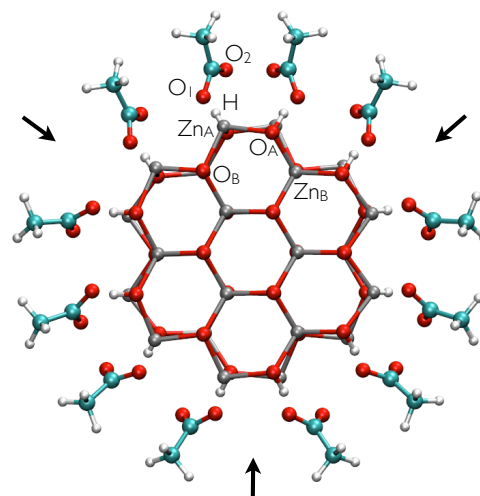


**Fig. 2** Cross-sectional view of the optimized structure of the AcOH-modified ZnO nanowire. Zinc, oxygen, hydrogen and carbon atoms are displayed by silver, red, white and cyan spheres, respectively. The black arrows indicate a ligand-free regions on the nanowire facets.

an eight-picoseconds (ps) MD run was performed. To verify if the considered supercell is large enough to sample a bulk water regime, we calculated the radial water density surrounding the nanowire during the MD run. Our results yield the standard water density of 1 g/cm<sup>3</sup> (data not shown), thus showing that the dimension of the supercell is indeed appropriate.

A snapshot of the corresponding trajectory at 8 ps is depicted in Figure 3. In order to describe the dynamics of the adsorbates, the  $\text{Zn}_A\text{-O}_1$  and  $\text{Zn}_A\text{-O}_2$  bond lengths, as well as the  $\text{H-O}_1$  hydrogen bond length are evaluated over time. The latter is shown in Figure 4 for every AcOH molecule in the supercell. The employed color code corresponds to that used in the snapshot of the trajectory (Figure 3) and the hydrogen bond lengths are plotted clockwise starting from the -COOH group with the gray-dyed carbon atom. The curves shown in Figure 4 can be split into two different groups according to the stability of the corresponding hydrogen bond. The first group comprises the plots in the first two columns (corresponding to adsorbates marked with colors gray, orange, green, black, purple and ochre), which yield very stable hydrogen bonds with an average length ranging approximately from 1.65 Å to 1.75 Å. The hydrogen bond lengths for the second group of adsorbates (third and fourth column in Figure 4) exhibit a stronger overall fluctuation. For the red-dyed ligand the fluctuations are especially large; the corresponding hydrogen bond length reaches values greater than 2.5 Å. The large fluctuations for the second group of ligands can be explained by their positions on the nanowire. They adsorb right next to the ligand-free region indicated with black arrows in Figure 3.



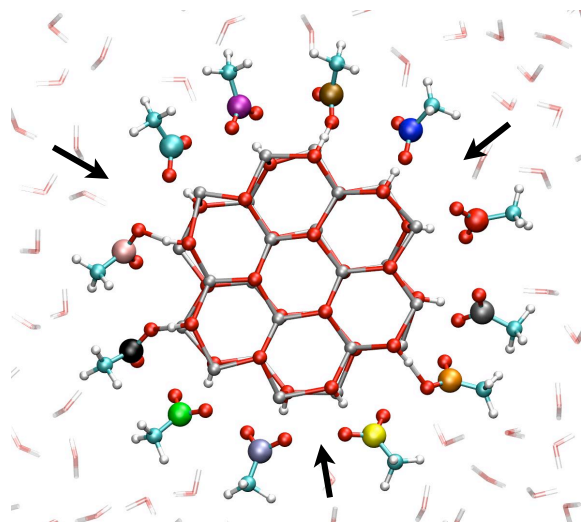


**Fig. 3** Snapshot of the molecular dynamics run at 8 ps for the fully-covered ZnO nanowire in aqueous medium. To distinguish between the twelve identical adsorbates, the carbon atom of the carboxylic group is shown in different colors. Zinc, oxygen and hydrogen atoms are displayed by silver, red and white spheres, respectively whereas the carbon atoms of the methyl groups has been represented by cyan spheres. For ease of viewing the bulk water is displayed transparent. The black arrows indicate the sites where bulk water is able to settle in.

Our results indicate that these ligand-free regions allow bulk water to approach the surface. These water molecules then interact with the carboxyl groups of the second group of adsorbates via formation of hydrogen bonds. From the analysis of the hydrogen bond lengths, it is therefore straightforward to identify a first influence of the bulk water on the adsorption of AcOH on the nanowires.

Similarly to the dry case, under wet conditions the -COOH group adsorbs in a bidentate mode as inferred from the analysis of the Zn-O bond length depicted in Figure 5. A common feature among the twelve plots is the formation of a bond between the surface Zn atom and one oxygen of the carboxyl group with an average bond length of about 2 Å. The distance between the second carboxyl oxygen and the Zn<sub>A</sub> site shows, on the other hand, strong fluctuations ranging from 2.2 to 3.2 Å. In general, the oxygen atom forming the stable Zn-O bond is not fixed during the MD run. In this sense the role of the two oxygens is interchangeable. Thus, we can conclude that the AcOH-ZnO interaction is dominated by a bond between one of the carboxyl oxygens and the Zn site with a bond length similar to that for Zn-O bonds in bulk ZnO. Analysis of the trajectory suggest that this tendency to a monodentate adsorption in the hydrated system is not mainly because of the interaction with water but rather due to the thermal fluctuations. Our results indicate, therefore, that the presence of bulk water

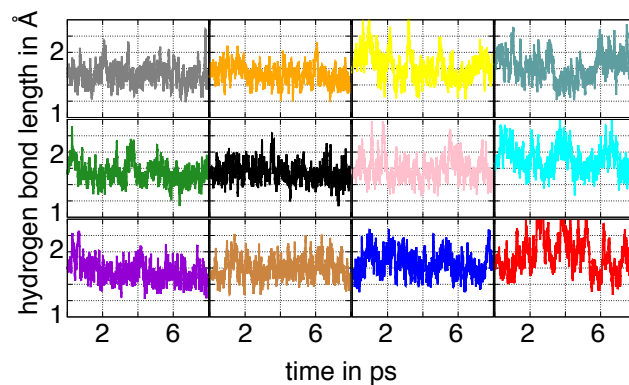


**Fig. 4** Hydrogen bond lengths between one of the oxygen atoms of the carboxyl group and the hydrogen atom transferred to the surface for the fully-covered ZnO nanowire during the simulation time. The color code corresponds to the one used in Figure 3.

appears to play only a minor role in the adsorption mode of the ligands for the fully covered ZnO nanowire.

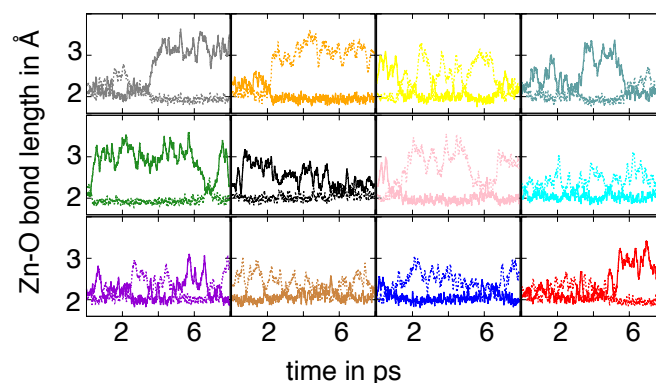


**Fig. 5** Bond lengths between the oxygen atoms of the carboxyl group, O<sub>1</sub> and O<sub>2</sub>, and the surface zinc atoms, Zn<sub>A</sub>, for the fully-covered ZnO nanowire during the simulation time. The color code corresponds to the one used in Figure 3 and the atom notation to the one employed in Figure 2.

To inspect if these results depend on the ligand coverage, we considered a second model where the nanowire is capped with a one-half monolayer of AcOH ( $\theta = 0.5$ ) in a bulk water environment. There are, doubtlessly, numerous ways to model the semi-covered ZnO nanowire, but as just the interaction between neighboring ligands is of interest here, we chose a configuration in which every second ligand was removed from the surface. The evaluation of the trajectory regarding the O<sub>1</sub>-H, Zn<sub>A</sub>-O<sub>1</sub> and Zn<sub>A</sub>-O<sub>2</sub> bonds is shown in Figure 6. The results for the hydrogen bond length exhibit strong fluctuations, especially for the molecules marked with the gray and yellow-dyed carbon, where the O<sub>1</sub>-H distances reach values greater than 3 Å. Analysis of the corresponding trajectory

shows that the bulk water is able to settle in between every neighboring AcOH molecules due to the newly available adsorption sites on the surface. These water molecules are able to form hydrogen bonds with the oxygen atoms of the carboxyl group. This interaction competes with the formation of hydrogen bonds between the molecule and the surface H atom. This finding is evinced from the analysis of the Zn-O bond lengths over time. Only the carboxyl oxygens of the pink- and green-dyed molecules alternately bind to the  $Zn_A$  site. For all other molecules the surface Zn atoms remain attached to the same molecular oxygen during the simulation. These results indicate that the adsorption of the ligands occurs in a monodentate mode. This reveals that the presence of water leads to an important stabilization of the anchor groups through formation of hydrogen bonds.

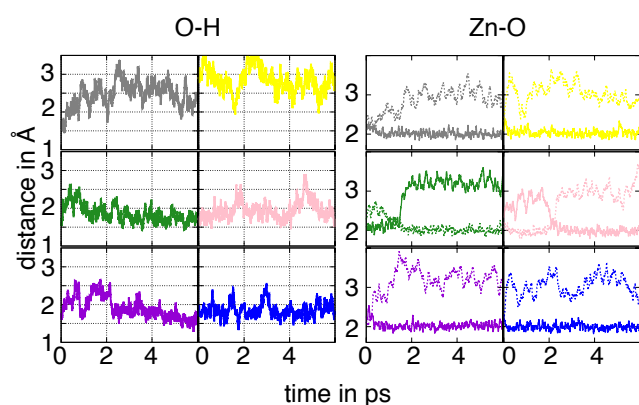


**Fig. 6**  $O_1$ -H hydrogen bond lengths (left) and  $Zn_A-O_1$  and  $Zn_A-O_2$  bond lengths (right) for the half-covered ZnO nanowire during the simulation time. The color code corresponds to the one used in Figure 3 and the atom notation to the one employed in Figure 2. Only the data for the adsorbed molecules are shown.

We finally consider a system in which all AcOH molecules are detached from the nanowire facets at the beginning of the simulation. This case corresponds to  $\theta = 0$ . The potential energy versus time for the three investigated coverages is shown in Figure 7. The energy of the system with  $\theta = 0$  was set to the zero of energy. The energy plots corresponding to  $\theta = 1$  and 0.5 show a similar trend and exhibit some overlap over nearly all time regimes. For  $\theta = 0$  the energy converges to a higher value during the MD run. To determine the adsorption energies for the considered systems we evaluated the energies obtained during the MD simulations in an approach similar to the one employed in a previous work on the adsorption of small molecules on  $TiO_2$  surfaces<sup>43</sup>. A Gaussian curve was fitted to the energy distribution obtained in the last picosecond of the simulation. The binding energies are then estimated as the difference between the Gaussian maxima of the investigated system and the system with  $\theta = 0$ . This leads to a total

binding energy of -8.84 eV for  $\theta = 1$ , which corresponds to an adsorption energy per ligand of -0.74 eV. For  $\theta = 0.5$  we find a binding energy of 6.84 eV and an adsorption energy per adsorbate of -1.14 eV. Thus, for both coverages the adsorption energies are smaller than for the system in the dry environment. Our results indicate that the fully-covered ZnO nanowire is the most stable system. This suggests that the modified nanostructure is stable against adsorption of liquid water under ligand-rich conditions. This is in agreement with recent experiments, which have demonstrated the successful functionalization of ZnO nanotips by immersing them in solutions of AcOH diluted to 2 mM per liter<sup>5</sup>. However, it should be borne in mind that an energy barrier needs to be overcome to replace molecules from the first water layer by AcOH. Investigation on energy barriers is out of the scope of this paper.

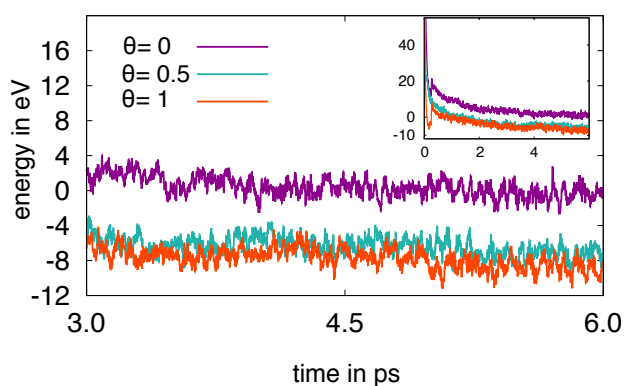


**Fig. 7** Energy distribution over the last picosecond of the simulation time obtained for the ZnO nanowire with the three considered coverages: full coverage ( $\theta=1$ ), half-coverage ( $\theta=0.5$ ) and total ligand desorption ( $\theta=0$ ). The energy of the ligand-free nanowire was set to the zero of energy. The inset shows the course of the energy over the entire simulation time.

## 4 Conclusions

We have investigated the adsorption of acetic acid on the facets of ZnO nanowires under dry conditions and in aqueous medium. For the former case, the geometry optimization of the adduct at 0 K indicated a strong bidentate adsorption of the ligand via two asymmetric O-Zn bonds. MD simulations of the system at 300 K and under wet conditions show small fluctuations of the bond length between one oxygen atom of the carboxyl group and the surface Zn atom around its optimized value at 0 K. In contrast, the distance from the other carboxylic oxygen to the Zn binding site was found to fluctuate considerably around larger values, thus indicating that this second attachment is weaker. This tendency to a monodenticity of the anchor groups is better seen for a system with half-covered nanowires. In this case, water occupies the now

available binding sites and interact with the adsorbed AcOH via H bonds, thus weakening one of the O-Zn bonds. The absolute value of the adsorption energy per adsorbate decreases considerably for the fully-covered nanowire under wet conditions compared to the dry case. Our results suggest that ZnO nanowires modified with acetic acid are still stable in aqueous solution at room temperature, as we have previously suggested in a more simplified model. Finally, we believe that our results motivate the investigation of migration barrier for the substitution of adsorbed water by AcOH which could help understand better the adsorption of functional groups and organic molecules on oxide surfaces in a wet environment.

## 5 Acknowledgement

This work was supported by the Deutsche Forschungsgemeinschaft under the program FOR1616. The Northern Germany supercomputing facility (HLRN) is acknowledged for computational resources.

## References

- 1 G. K. Mor, K. Shankar, M. Paulose, O. Varghese and C. Grimes, *Nano Lett.*, 2006, **6**, 215.
- 2 E. Galoppini, J. Rochford, H. Chen, G. Saraf, Y. Lu, A. Hagfeldt and G. Boschloo, *The Journal of Physical Chemistry B*, 2006, **110**, 16159–16161.
- 3 K. Zhu, N. R. Neale, A. Miedaner and A. J. Frank, *Nano Lett.*, 2007, **7**, 69.
- 4 G. Benkő, J. Kallioinen, J. E. I. Korppi-Tommola, A. P. Yartsev and V. Sundström, *J. Am. Chem. Soc.*, 2002, 489.
- 5 O. Taratula, E. Galoppini, D. Wang, D. Chu, Z. Zhang, H. Chen, G. Saraf and Y. Lu, *J. Phys. Chem. B*, 2006, **110**, 6506.
- 6 S. Blumstegel, H. Glowatzki, S. Sadofev, N. Koch, S. Kowarik, J. P. Rabe and F. Henneberger, *Phys. Chem. Chem. Phys.*, 2010, **12**, 11642.
- 7 S. Rani, P. K. Shishodia and R. M. Mehra, *Journal of Renewable and Sustainable Energy*, 2010, **2**, 043103.
- 8 K. Keis, J. Lindgren, S.-E. Lindquist and A. Hagfeldt, *Langmuir*, 2000, **16**, 4688–4694.
- 9 K. Keis, E. Magnusson, H. Lindström, S.-E. Lindquist and A. Hagfeldt, *Solar Energy Materials and Solar Cells*, 2002, **73**, 51–58.
- 10 T. Dentani, K. ichi Nagasaka, K. Funabiki, J.-Y. Jin, T. Yoshida, H. Minoura and M. Matsui, *Dyes and Pigments*, 2008, **77**, 59–69.
- 11 H. Gao, G. Fang, M. Wang, N. Liu, L. Yuan, C. Li, L. Ai, J. Zhang, C. Zhou, S. Wu and X. Zhao, *Materials Research Bulletin*, 2008, **43**, 3345–3351.
- 12 I. Gonzalez-Valls and M. Lira-Cantu, *Energy Environ. Sci.*, 2009, **2**, 19–34.
- 13 E. Guillén, C. Fernández-Lorenzo, R. Alcántara, J. Martín-Calleja and J. Anta, *Solar Energy Materials and Solar Cells*, 2009, **93**, 1846–1852.
- 14 W.-H. Chiu, C.-H. Lee, H.-M. Cheng, H.-F. Lin, S.-C. Liao, J.-M. Wu and W.-F. Hsieh, *Energy Environ. Sci.*, 2009, **2**, 694–698.
- 15 N. M. Gómez-Ortíz, J. Idígoras, E. Guillén, A. Hernández, A. Sastre-Santos, F. Fernández-Lázaro, J. Anta and G. Oskam, *J. Photochem. Photobiol. A Chem.*, 2013, **264**, 26–33.
- 16 M. Saito and S. Fujihara, *Energy Environ. Sci.*, 2008, **1**, 280–283.
- 17 N. Koide, R. Yamanaka and H. Katayama, *MRS Proceedings*, 2009, **1211**, R12–R22.
- 18 S. Kuehn, S. Friede, S. Sadofev, S. Blumstengel, F. Henneberger and T. Elsaesser, *Applied Physics Letters*, 2013, **103**, 191909.
- 19 Y. Cao, E. Galoppini, P. I. Reyes and Y. Lu, *Langmuir*, 2013, **29**, 7768–7775.
- 20 K. Yao, L. Chen, Y. Chen, F. Li and P. Wang, *The Journal of Physical Chemistry C*, 2012, **116**, 3486–3491.
- 21 S. K. Hau, Y.-J. Cheng, H.-L. Yip, Y. Zhang, H. Ma and A. K.-Y. Jen, *ACS Applied Materials & Interfaces*, 2010, **2**, 1892–1902.
- 22 X. Tian, J. Xu and W. Xie, *J. Phys. Chem. C*, 2010, **114**, 3973–3980.
- 23 A. Lenz, L. Selegård, F. Soderlind, A. Larsson, P. O. Holtz, K. Uvdal, L. Ojamae and P.-O. Kall, *The Journal of Physical Chemistry C*, 2009, **113**, 17332–17341.
- 24 O. Taratula, E. Galoppini, R. Mendelsohn, P. I. Reyes, Z. Zhang, Z. Duan, J. Zhong and Y. Lu, *Langmuir*, 2009, **25**, 2107–2113.
- 25 A. Gupta, B. C. Kim, E. Edwards, C. Brantley and P. Ruffin, *Adv. Mat. Res.*, 2012, **567**, 228–231.
- 26 G. J. Ehler and H. A. Sodano, *ACS Applied Materials & Interfaces*, 2009, **1**, 1827–1833.
- 27 J. Chen, R. E. Ruther, Y. Tan, L. M. Bishop and R. J. Hamers, *Langmuir*, 2012, **28**, 10437–10445.
- 28 N. H. Moreira, A. L. da Rosa and T. Frauenheim, *Appl. Phys. Lett.*, 2009, **94**, 193109.
- 29 N. H. Moreira, A. Dominguez, T. Frauenheim and A. L. da Rosa, *Phys. Chem. Chem. Phys.*, 2012, **14**, 15445–15451.
- 30 A. Dominguez, N. H. Moreira, G. Dolgonos, A. L. Rosa and T. Frauenheim, *J. Phys. Chem. C*, 2011, **115**, 6491–6495.
- 31 G. Kresse and J. Hafner, *Phys. Rev. B*, 1993, **47**, 558–561.
- 32 G. Kresse and J. Hafner, *Phys. Rev. B*, 1994, **49**, 14251–14269.
- 33 G. Kresse and J. Furthmüller, *Computational Materials Science*, 1996, **6**, 15–50.
- 34 G. Kresse and J. Furthmüller, *Phys. Rev. B*, 1996, **54**, 11169–11186.
- 35 J. Perdew, K. Burke and M. Ernzerhof, *Phys. Rev. Lett.*, 1996, **77**, 3865–3868.
- 36 J. P. Perdew, K. Burke and M. Ernzerhof, *Phys. Rev. Lett.*, 1997, **78**, 1396–1396.
- 37 P. E. Blöchl, *Phys. Rev. B*, 1994, **50**, 17953–17979.
- 38 G. Kresse and D. Joubert, *Phys. Rev. B*, 1999, **59**, 1758–1775.
- 39 H. J. Monkhorst and J. D. Pack, *Phys. Rev. B*, 1976, **13**, 5188–5192.
- 40 J. D. Pack and H. J. Monkhorst, *Phys. Rev. B*, 1977, **16**, 1748–1749.
- 41 CPMD, <http://www.cpmd.org/>, Copyright IBM Corp 1990-2008, Copyright MPI für Festkörperforschung, Stuttgart 1997-2001.
- 42 D. Vanderbilt, *Phys. Rev. B*, 1990, **41**, 7892–7895.
- 43 S. Koppen, O. Bronkalla and W. Langel, *J. Phys. Chem. C*, 2008, **112**, 13600–13606.